

Two-Step Functionalization of Neutral and Positively Charged Thiols onto Citrate-Stabilized Au Nanoparticles

Shu-Yi Lin, Yi-Ting Tsai, Chien-Chih Chen, Chia-Mei Lin, and Chun-hsien Chen*

Department of Chemistry, National Tsing Hua University, Hsinchu, Taiwan 30013, ROC

Received: August 5, 2003; In Final Form: November 19, 2003

We propose a two-step approach to functionalize gold nanoparticles prepared by reducing tetrachloroauric acid by trisodium citrate in water. The chloride and citrate physisorbed on the gold nanoparticles are first displaced by thioctic acid (TA), which is then exchanged by thiols containing the desired functionality during the second step. TA bears a carboxylate group and disulfide; at high pH, the negative charge of the former stabilizes gold nanoparticles and the disulfide develops two S–Au bonds, retarding the desorption kinetics upon further functionalization. The slow kinetics of TA desorption is crucial to establishing sufficient steric stabilization for the gold core while losing electrostatic stabilization. Successful attachment of carboxylate, crown ether, cyclodextrin, pyridine, and amino functionalities is verified by surface sensitive techniques. In most cases, ca. 80% of the TA molecules are displaced. The nanoparticles are stable under solution pH where the surface group is ionized. Although at certain solution acidities, the gold sols have difficulty carrying charges and appear flocculated, the nanoparticles become dispersive after being centrifuged and redissolved in suitable buffer solutions, which indicates the successful protection of the gold cores by steric stabilization.

Introduction

Surface functionalization of gold nanoparticles is a focus of current research interest in fundamentally understanding their physical chemistry and receptor-based sensor applications.^{1–14} A popular two-phase synthesis of the functionalized nanoparticles initiated by Schiffrin et al. involves thiol–gold chemistry and transfer of the organothiol-stabilized gold nanoparticles from an aqueous to organic phase.¹⁵ This method produces particles smaller than 5 nm in diameter and thus termed MPC (monolayer protected clusters).¹⁶ Because of their similarity to SAMs (self-assembled monolayers), MPCs can use readily available modification schemes outlined in parallel literature examples to engineer interfacial structures.^{16–24} In comparison to nanoparticles protected by ionic and polymeric stabilizers,^{25,26} MPCs, by taking advantage of strong thiol–gold interactions and van der Waals attractions of neighboring molecules, exhibit superior stability, a prerequisite for practical applications. However, from the aspect of optical sensing that relies on the chromophoric characteristics of nanoparticles whose molar extinction coefficient of the surface plasmon band is proportional to their volume,^{27,28} a satisfactory sensitivity would demand a larger particle size than MPCs have and thus require another synthetic strategy.

Alternatively, gold nanoparticles bearing both excellent optical sensitivity and stability can be, in principle, obtained first by synthesis of suitably sized nanoparticles, followed by chemisorption of thiols onto the spheres of the colloidal gold. To facilitate assembly of the subsequent organosulfur protection layer, the stabilizers employed in the first step should be readily displaced and be small anionic species. However, upon chemisorption of thiols, the desorption of charged species sacrifices the electrostatic stability and sometimes causes irreversible aggregation.^{29–32} For example, chloride and citrate-stabilized nanoparticles are prepared by reducing tetrachloroauric acid with

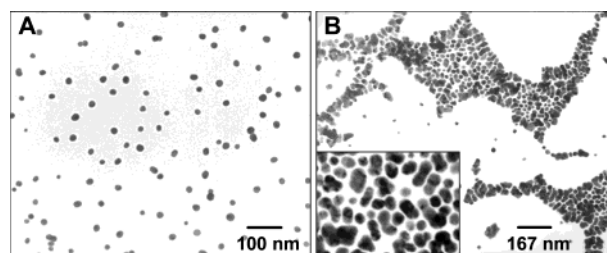


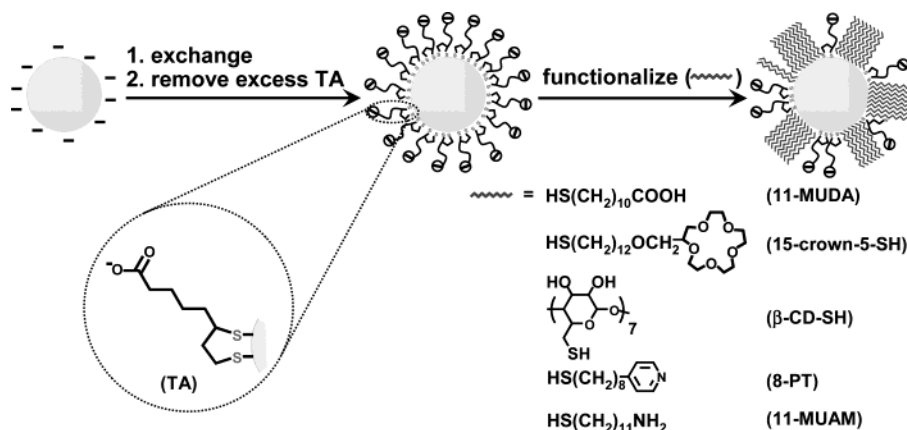
Figure 1. TEM micrographs of citrate-stabilized gold nanoparticles (A) before and (B) after addition of 15-crown-5-SH. The modification was carried out by mixing 4 mL of colloidal gold (1.3 mg/mL) and 6 drops of the thiol (2 mg/mL in ethanol).

trisodium citrate in water.^{5,33,34} This method features controllable sizes on the order of tens of nanometers by adjustment of the gold-to-citrate ratio. Particles prepared in this fashion are commercially available in various monodisperse sizes.³³ Modification of gold nanoparticles is carried out by adding ω -functionalized thiol into the aqueous solution of colloidal gold. When the thiol is not negatively charged, colloidal gold can easily undergo irreversible aggregation.^{29–32} Parts A and B of Figure 1 show, respectively, micrographs taken before and after adding a neutral thiol, 2-(12-mercaptododecyloxy)methyl-15-crown-5 ether (15-crown-5-SH), into a solution of citrate-stabilized gold nanoparticles. The solution often turns steel blue immediately, indicative of particle aggregation^{28,29} causing a red shift of surface plasmon bands. The fusion of gold cores^{30,31} revealed in the inset of Figure 1B suggests a loss of the electrostatic stability during displacement of the absorbed anions by the neutral crown-thiol. Although gold nanoparticles may stay dispersive due to the electrostatic and steric stability provided by the anionic charges and the organosulfur monolayers, respectively, it is evidently not trivial to simultaneously preserve the charges and assemble the protective monolayer.

Aslan and Perez-Luna introduced an approach that developed steric stabilization of gold nanoparticles by mixing them with Tween 20 prior to modifying the carboxylate-terminated al-

* To whom correspondence should be addressed. Phone: (+886) 3-573-7009. Fax: (+886) 3-571-1082. E-mail: chhchen@mx.nthu.edu.tw.

SCHEME 1. Illustration of the Two-Step Modification



kanethiol (11-mercaptopundecanoic acid, 11-MUDA).³² Tween 20, a nonionic surfactant containing oligo(ethylene glycol) moieties, physisorbed on gold surfaces and prevented the nanoparticles from aggregating in the subsequent reaction. 11-MUDA penetrated through the Tween 20 layer and displaced the underlying anionic citrate and chloride. When the new protection layer had been established, Tween 20 was removed and the gold nanoparticles remained stable. After analyzing the success of this example, we believe that the key is to ensure the assembly of the thiol protection layer by slowing down removal of the charged species. Proposed in this study is the two-step strategy illustrated in Scheme 1. The first step is displacement of citrate and chloride by a relatively short and negatively charged thiol that exhibits strong interactions with gold and thus provides sufficient time to build up densely packed monolayers in the second step. As illustrated in the second step of Scheme 1, this concept is assessed by functionalization of nanoparticles using negatively charged (carboxylate), neutral (crown and cyclodextrin), and positively charged (pyridinium and ammonium) moieties. To the best of our knowledge, this is the first study in aqueous solution that converts citrate-stabilized gold nanoparticles into oppositely charged ones. It successfully resolves the aforementioned dilemma of organizing steric stabilization at the cost of losing electrostatic stabilization.

Experimental Section

Materials and Buffer Solutions. All chemicals were reagent grade and used as received. 2-(12-Mercaptododecyloxy)methyl-15-crown-5 ether (15-crown-5-SH),³⁵ per-6-thio- β -cyclodextrin (β -CD-SH),³⁶ and 11-mercaptopundecylamine (11-MUAM)³⁷ were synthesized according to procedures in the literature. 8-(4-Pyridyl)octanethiol (8-PT) was a gift from Dr. Yu-Tai Tao (Institute of Chemistry, Academia Sinica, Taipei). All buffer solutions were 10 mM and prepared as follows: pH 2–4, phosphoric acid/sodium phosphate monobasic; pH 5, acetic acid/sodium acetate; pH 6 and pH 7, sodium phosphate monobasic/sodium phosphate dibasic; pH 8 and pH 9, sodium phosphate dibasic; pH 11, sodium carbonate. The final buffer pH was monitored by a pH meter (Orion 410) and fine-tuned by droplet addition of HCl, NaOH, or H_3PO_4 . Millipore-Q water ($18.2 \text{ M}\Omega\cdot\text{cm}^{-1}$) was used to prepare all solutions.

Preparation and Modification of Gold Sols. Gold colloids were prepared by sodium citrate reduction of HAuCl_4 as in those methods developed by Natan and co-workers.^{33,34} All glassware was thoroughly cleaned with aqua regia (3:1 HCl/HNO_3) and rinsed with Millipore-Q water prior to use. The average diameter measured by transmission electron microscopy (TEM, Hitachi,

H-7500) was $17.1 \pm 3.0 \text{ nm}$ with Scion Image Beta Release 2 (available at www.scioncorp.com). In search of suitable thiols for step one (Scheme 1), 0.40 mL of carboxylate-terminated thiols (i.e., 2-mercaptoethanoic acid (MEA), 3-mercaptopropanoic acid (MPA), thioctic acid (TA), and 11-mercaptopundecanoic acid (11-MUDA)) were added to 4.0 mL of citrate-stabilized gold sols whose basicities were preadjusted to pH 11 by 40 μL of 0.5 M NaOH. High basicity is important in reinforcing static stabilization. The gold sols were stirred overnight (12–18 h). The carboxylate-functionalized nanoparticles were then centrifuged for 10 min (at 15700g, 10 $^\circ\text{C}$, Sorvall, Biofuge Stratos, Germany), followed by decantation of supernatants. MEA- and MPA-functionalized gold sols generally appeared purplish after being centrifuged, suggesting insufficient steric stabilization.

For step two, the purified TA-stabilized gold nanoparticles were redissolved in Millipore-Q water. The solution was adjusted to pH 11 by NaOH. A 0.40 mL aliquot of the ω -substituted alkanethiols solution, except 11-MUAM, was mixed with 4.0 mL of TA-stabilized gold sols. The mixture was stirred overnight ($\sim 18 \text{ h}$). In the case of 11-MUAM, TA-stabilized gold nanoparticles were dissolved in Millipore-Q water (without electrolytes). After 0.4 mL of 11-MUAM was mixed with 4.0 mL of TA-stabilized gold sol, the solution immediately became dark purple. One hour later, 0.40 mL of 1 M HCl was added and the gold sol turned red in about 3–4 h. The overall stirred time was about 18 h. Due to poor solubility of thiols in water, thiol solutions were prepared differently: 11-MUDA, 10 mM/ethanol; 15-crown-5-SH, 4.4 mM/ethanol; β -CD-SH, 7 mM/water; 8-PT, 10 mM/ethanol; 11-MUAM, 4 mM/ethanol. Excess thiols were removed by being centrifuged twice for 10 min (at 15700g, 10 $^\circ\text{C}$), followed by decantation of supernatants. Surface functionalities were characterized by TEM, FTIR (Perkin-Elmer, Spectrum 2000), and XPS (Physical Electronics, ESCA PHI 1600).

Determination of Flocculation Parameter. The flocculation parameter was defined by integrating the absorbance spectrum between 600 and 800 nm.²⁹ The spectra were obtained by a Unicam UV 300 spectrophotometer, and the gold sols were thermostated at 20 $^\circ\text{C}$ (Thermo Spectronic, Single Cell Peltier). Centrifugation twice for 10 min (at 15700g, 10 $^\circ\text{C}$) was employed to isolate the functionalized gold nanoparticles from the excess thiols in step two. The flocculation parameters were measured ca. 2 min after adding the purified nanoparticles into 3 mL buffer solutions. For a better comparison, the intensity of the surface plasmon band for all gold sols was fixed at 0.18 AU, equivalent to 18.8 $\mu\text{g}/\text{mL}$.

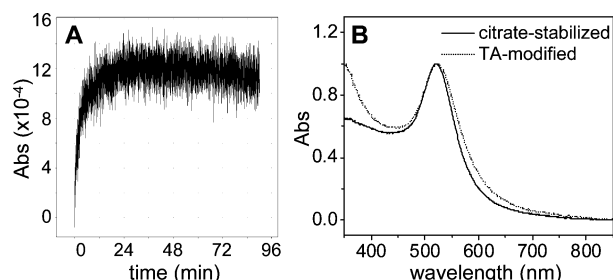


Figure 2. (A) Adsorption kinetics of TA onto colloidal gold, measured by monitoring absorbance at 550 nm. (B) UV/vis spectra of citrate-stabilized (solid line) and TA-stabilized (dash line) gold sols. The spectra were obtained in deionized water, similar to the protocol developed by Aslan and Perez-Luna.³²

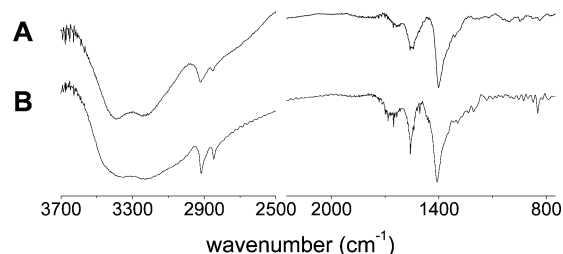


Figure 3. Transmission FTIR spectra of carboxylate-functionalized nanoparticles. (A) TA-stabilized and (B) 11-MUDA-stabilized gold nanoparticles in a KBr pellet. The latter were prepared via the two-step method, and the spectrum was indistinguishable from that obtained by directly mixing 11-MUDA with citrate-stabilized nanoparticles.

Results and Discussion

Suitability Evaluation of Small Thiols for the First Step.

For the practical applicability of the first step, only commercial compounds are examined because of their ready availability. The candidates are carboxylate-terminated thiols, including MEA, MPA, TA, and 11-MUDA, which carry a negative charge under sufficient solution basicity. After adding these thiols into basic gold sols, the colloidal solutions for all cases remain red and show no sign of aggregation, a result of charge preservation upon displacement of the adsorbed citrate by the anionic thiols. However, only TA-stabilized nanoparticles are effective for the subsequent functionalization. Therefore, modification procedures and characterization will be described in detail only for TA-stabilized nanoparticles.

Figure 2A shows the exchange kinetics of TA in deionized water by monitoring absorbance changes at 550 nm where absorbance is strongly affected by the change of the local refractive index at the modifier–nanoparticle interface.^{10,32} The modification of TA on gold nanoparticles reaches equilibrium in about 20 min. Nevertheless, we choose to mix TA with citrate-stabilized gold sol overnight (~ 12 h). Figure 2B shows the optical absorption spectra of colloidal gold before and after modifying TA. The surface plasmon band exhibits a slight red shift associated with the attachment of TA. Figure 3A is a transmission IR spectrum of TA-stabilized gold nanoparticles after being purified by centrifugation twice, lyophilized, and prepared in a KBr pallet. The absorption around 3250 cm^{-1} is a result of residual moisture within the dried nanoparticles. The peaks at 2925 , 2850 , 1561 , and 1401 cm^{-1} are vibrational modes of $\nu_{\text{asy}}(\text{CH}_2)$, $\nu_{\text{sym}}(\text{CH}_2)$, $\nu_{\text{asy}}(\text{CO}_2^-)$, and $\nu_{\text{sym}}(\text{CO}_2^-)$, respectively. The spectrum demonstrates the successful attachment of TA onto gold nanoparticles because the SH band around 2550 cm^{-1} is undetectable and because the CH stretches of $\nu_{\text{asy}}(\text{CH}_2)$ and $\nu_{\text{sym}}(\text{CH}_2)$ are strong in Figure 3A and invisible for citrate-stabilized gold nanoparticles.⁸ XPS spectra (X-ray photoelectron

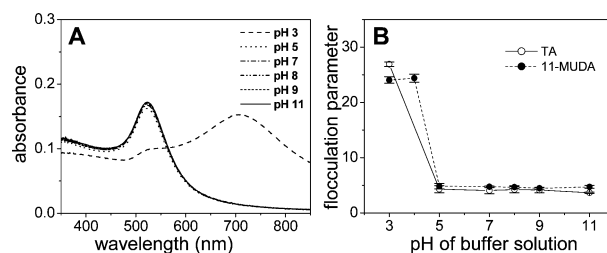


Figure 4. Stability of carboxylate-functionalized gold nanoparticles. (A) UV/vis spectra of TA-stabilized colloidal gold at pH 3 \sim 11. (B) Flocculation parameter (extinction \times nm) of the gold sols as a function of buffer pH.

spectroscopy, not shown) also reveal the S_{2p} band and confirm that TA displaces citrate and stabilizes gold nanoparticles in the first step.

The stability of the gold nanoparticles is evaluated by integrating the area under the absorbance curve between 600 and 800 nm, on the basis of the flocculation parameter defined by Whitesides et al.^{29,32,38} Figure 4A shows the UV/vis spectra obtained after introducing buffer solutions into twice-centrifuged TA-stabilized gold nanoparticles. Preparation details of the buffer solutions are described in the Experimental Section. The spectra appear identical except the one measured at pH 3 in which the surface plasmon peak at 523 nm is reduced and a broad band from 600 to 800 nm is raised. The plot of flocculation parameter against solution pH (Figure 4B, open circles) manifests that the nanoparticles are dispersive when the solution basicity is stronger than pH 5. When the flocculated nanoparticles are isolated from the low pH buffer by centrifugation and redissolved in a higher pH buffer ($\text{pH} \geq 5$), the gold sol again becomes dispersive and turns red. The UV/vis spectra and TEM micrographs show no indication of aggregation or fusion of metal cores. The flocculation at pH 3 is, most likely, induced by interparticular H-bonding between carboxylate groups.^{39–41}

For MEA and MPA, after mixing with citrate-stabilized gold sols, the solutions do not exhibit any sign of instability. Prior to the second step (Scheme 1), the thiol-stabilized gold nanoparticles are centrifuged twice to remove the unattached thiols. However, the resuspended solutions of MEA- and MPA-modified nanoparticles appear purplish. TEM micrographs show fusion of gold cores. These results demonstrate that thiols with very short methylene chains do not establish sufficient steric stabilization to protect the nanoparticles against aggregation. On the other hand, 11-MUDA has relatively more methylene units and the IR spectra of 11-MUDA-stabilized nanoparticles (similar to Figure 3B, not shown) reveal that $\nu_{\text{asy}}(\text{CH}_2)$ is centered at 2918 cm^{-1} , indicative of a highly crystalline and primarily trans-zigzag extended polymethylene monolayer.⁴² However, further exchange with other ω -functionalized thiols does not take place on 11-MUDA-stabilized nanoparticles, suggesting that long-chain thiols protect the nanoparticles too strongly to be suitable for the first step.

Structural Characterization of Two-Step Functionalized Nanoparticles. The second step illustrated in Scheme 1 involves adding the listed thiols into a stirred TA-stabilized gold sol. The evolution of absorbance at 550 nm indicates that exchange of TA by 11-MUDA is far slower than that of citrate-stabilized gold nanoparticles. It requires at least 5.5 h to reach a state where change in absorbance appears less distinctive. This is attributed to two thiol–gold bindings per thioctic acid. The slow exchange helps the neutral and nitrogen-containing thiols to build up steric stabilization for nanoparticles upon losing anionic TA. To enhance electrostatic stabilization, the solution basicity

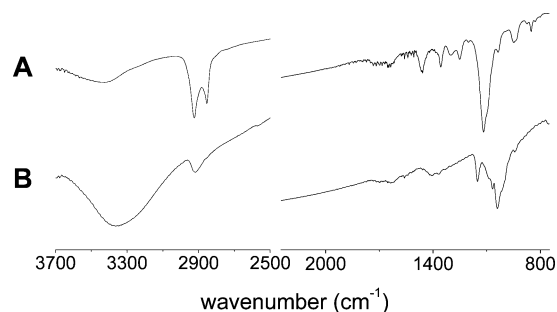


Figure 5. Transmission FTIR spectra of TA-stabilized nanoparticles exchanged by neutral thiols. (A) 15-crown-5-S- and (B) β -CD-S-functionalized gold nanoparticles in a KBr pellet.

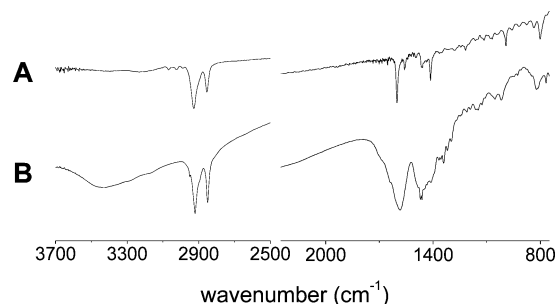


Figure 6. Transmission FTIR spectra of potentially positive-charged nanoparticles. (A) 8-PT- and (B) 11-MUAM-functionalized gold nanoparticles in a KBr pellet.

is adjusted to pH 11. 11-MUAM is an exception. TA-stabilized gold nanoparticles are prepared in Millipore-Q water (without electrolytes) for the amino-terminated thiol. Upon mixing, the solution becomes dark purple. One hour later, 0.40 mL of 1 M HCl is added and the gold sol again turns red gradually in about 3–4 h. The dark purple color indicates flocculated gold sols due to formation of interparticular H-bonding between amino groups at high pH, suggesting that a certain fraction of TA is exchanged by 11-MUAM. The solutions are stirred overnight. After being centrifuged twice to remove free thiols and redissolved in water, the gold sols remain red and dispersive in all cases.

The nanoparticles for transmission IR measurements are centrifuged twice and lyophilized. Figures 3B, 5, and 6 represent modification of nanoparticles by negatively, neutrally, and positively charged thiols, respectively. Successful functionalization is confirmed by the vibrational characteristics of the terminal groups present at 1409 ($\nu_{\text{sym}}(\text{CO}_2^-)$) and 1559 ($\nu_{\text{asy}}(\text{CO}_2^-)$) cm^{-1} for carboxylate (11-MUDA, see Figure 3B); 949, 1117, 1252, 1300, 1357, and 1458 cm^{-1} for crown moiety (Figure 5A); 1040, 1067, 1151, 1366 cm^{-1} ($\nu_{\text{str}}(\text{CO})$) for cyclodextrin (Figure 5B); ring vibrations at 1414, 1557, and 1602 cm^{-1} for pyridinium (Figure 6A); 1064 ($\nu_{\text{str}}(\text{NH}_2)$) and 1585 ($\nu_{\text{def}}(\text{NH}_2)$) cm^{-1} for amino (Figure 6B). The $\nu_{\text{asy}}(\text{CH}_2)$ vibrations for 11-MUDA-, 15-crown-5-S-, and 11-MUAM-modified nanoparticles reside respectively at 2918, 2920, and 2920 cm^{-1} , indicative of crystallinity for the relatively long thiols. The monolayers are disorganized for relatively short thiols such as TA- and 8-PT-modified nanoparticles whose $\nu_{\text{asy}}(\text{CH}_2)$ peaks are centered at 2925 and 2923 cm^{-1} , respectively. For β -CD-S-modified nanoparticles, the presence of SH absorption at ~ 2560 cm^{-1} shows that some of the seven thiols per β -CD-SH are unattached. This is because of the difficulty in displacing TA by β -CD-SH due to its bulky size and the lack of intermolecular van der Waals attractions. For all other cases, the SH vibrational mode is absent, confirming the attachment of the ω -functionalized thiols on gold. The broad band appearing

TABLE 1: XPS Measurements of the ω -Functionalized Nanoparticles Prepared by the Two-Step Method

ω -functionalized thiols	binding energy ^a (eV)			abundance ratio ^b		exchange ratio ^c (%)
	S _{2p3/2}	O _{1s}	N _{1s}	O/S	N/S	
11-MUDA	163.6	531.3		2.06		$\sim 100 \pm 2$
15-crown-5-SH	163.3	533.3		4.21		64 ± 3
β -CD-SH	163.9	532.9		2.99		67 ± 2
8-PT	163.4	531.7	399.6	0.31	0.69	69 ± 3
11-MUAM	163.5	532.2	400.5	0.38	0.66	64 ± 3

^a The nanoparticles were centrifuged twice and drop-cast on thermally evaporated gold substrate. ^b Calculation of the abundance ratio was based on peak area multiplied by the corresponding atomic sensitive factor. ^c The exchange ratio represents the percentage of thiol legs of the ω -functionalized thiols out of the overall thiol legs on nanoparticles, roughly representative of the TA exchanged in the second step.

at 3000–3600 cm^{-1} arises from residual moisture, very hard to remove due to the hygroscopic features of the modified nanoparticles. Note also that all the IR spectra exhibit, to a certain degree, symmetric (~ 1400 cm^{-1}) and asymmetric (~ 1550 cm^{-1}) peaks of carboxylates, suggesting that TA monolayers are not completely displaced.

To clarify the degrees of exchange at the equilibrium state monitored by UV/vis, the modified nanoparticles are examined by XPS, and the results are summarized in Table 1. The peak positions are generally in good accordance with their oxidation states. The relatively high binding energy of S_{2p3/2} for β -CD-SH is ascribed to the contribution of free thiols revealed from IR measurements (Figure 5B). The abundance ratio is estimated by taking the peak areas and atomic sensitivity factors into consideration. From the abundance ratio and the numbers of sulfur, oxygen, and nitrogen atoms per molecule, the percentages of the ω -functionalized thiols to total number of thiols per nanoparticle are estimated to be roughly 100, 78, 36, 82, and 78%, respectively, for 11-MUDA-, 15-crown-5-S-, β -CD-S-, 8-PT-, and 11-MUAM-stabilized nanoparticles. 11-MUDA completely displaces TA probably because they both carry anionic carboxylate and the assembly of monolayers is thermodynamically in favor of 11-MUDA whose linear and longer chain generates stronger intermolecular attractions and better packing. In the case of β -CD-SH, the percentage (36%) appears less than half of the others due to the bulky shape and seven thiol legs per molecule. Therefore, percentages derived from fractionation of molecules on nanoparticles could be misleading. The exchange ratio listed in Table 1 is revised by using the number of thiol legs attached during the second step relative to that of total thiol legs on the gold nanoparticle. This expression roughly represents the percentage of TA exchanged. The exchange ratios fall in the range 64–69% for neutral and positively charged thiols.

Exchange experiments where surface-bound thiols are displaced by excess free thiols in solution have been carried out both on flat gold substrate^{43–45} and on faceted MPCs.^{16,46–48} Although in these studies the experimental conditions are very different in molar ratios of free to surface-bound molecules and in properties of solvents and molecules, one common feature is that the exchange reaction generally involves both a fast and a slow step. The fast step takes place at defects where free thiols can reach the gold surface relatively easily, such as domain boundaries on the flat substrate and edge and vertex sites on the MPCs. At terraces or domains where the molecules are tightly packed, the kinetics is so slow that the exchange remains incomplete for reactions taking longer than 10 days.^{43–45} In this current study, the functionalization time for the nanoparticles measured in Table 1 was about 18 h. The exchange ratios are

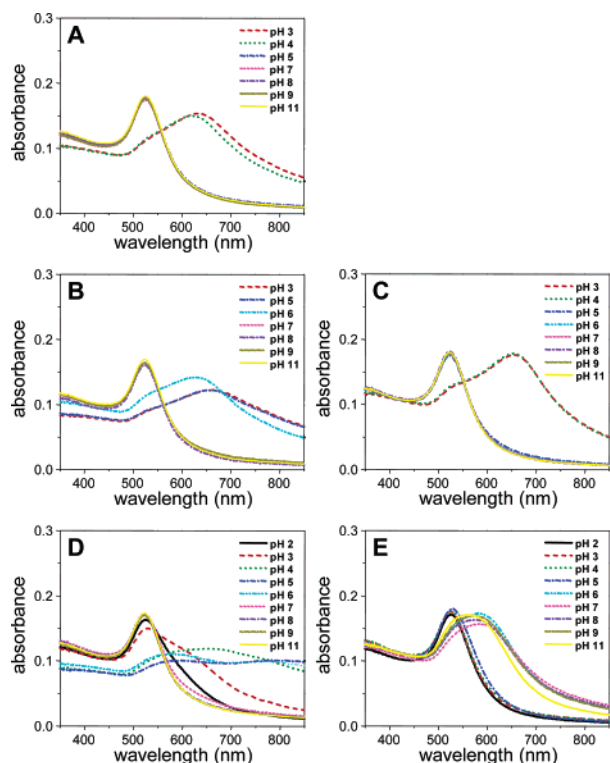


Figure 7. UV/vis spectra obtained at pH 2–11 for colloidal gold functionalized by (A) 11-MUDA, (B) 15-crown-5-SH, (C) β -CD-SH, (D) 8-PT, and (E) 11-MUAM. (For coding see Scheme 1.)

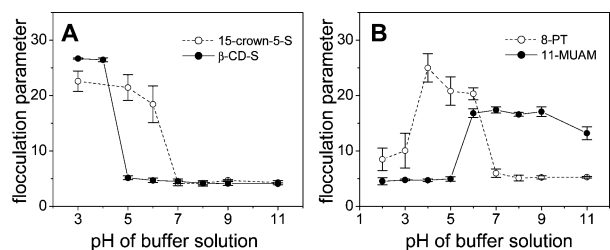


Figure 8. Stability of gold nanoparticles functionalized by (A) neutral and (B) potentially positive-charged thiols. The flocculation parameters (extinction \times nm) were measured by introducing the corresponding buffer solution into twice-centrifuged nanoparticles.

far larger than those on flat gold^{43,44} and about 5–10% smaller than those on MPCs (2 nm in diameter),⁴⁶ qualitatively consistent with their defect or domain sizes. The exchange mechanism of this functionalization scheme should be quite similar to those studied on flat surfaces and on MPCs.

Stability of Gold Nanoparticles after Two-Step Functionalization. Stability of the two-step functionalized nanoparticles is evaluated by the flocculation parameter (vide supra). Although the nanoparticles appear purplish or flocculated within particular pH ranges, the gold sols become red and dispersive after being centrifuged and redissolved in suitable buffer solutions. The absorption spectra following the functionalization as shown in Figure 7 are a strong evidence that the two-step functionalization is successful. Fusion of gold cores is not taking place because of the steric stabilization. Figure 4B shows that the behavior of 11-MUDA-functionalized nanoparticles is very similar to that of TA-stabilized ones, dispersive at solution basicities stronger than pH 5. The neutral thiol-functionalized nanoparticles are stable at high pH (Figure 8A), a result of the presence of residual TA, which is revealed by IR and XPS measurements. The pH limit of stable gold sols for β -CD-S-functionalized nanoparticles (pH 5) is lower than that for 15-crown-5-S-functionalized ones

(pH 7) because TA molecules on the latter are embedded within the methylene chains whereas the molecules are exposed to the solution on the former.

The significance of the two-step methodology is demonstrated in Figure 8B where the positively charged nanoparticles functionalized by 8-PT and 11-MUAM are stable at low pHs. The stable pH range for 11-MUAM-functionalized gold sols is up to pH 5 and is wider than that of 8-PT-functionalized gold sols, consistent with the fact that the pK_a of the amino group (~ 10) is larger than that of pyridinium (~ 5). The transient pH between dispersive and flocculated states is attributed to the surface pK_a , 3–5 pH units lower than the corresponding aqueous pK_a . This shift is due to the difficulty of stabilizing the high charge density at the pyridinium- or ammonium-terminated interface.^{40,49} At solution basicity stronger than pH 6, 11-MUAM-functionalized gold sols become flocculated. This is due to the formation of interparticular H-bonding, similar to the carboxylate-terminated gold nanoparticles in acidic solutions (Figure 4B).⁵⁰ Because 11-MUAM is longer than TA, the carboxylate group of TA is embedded within the 11-MUAM monolayer and affects the stability of gold sols at high pHs. For example, upon flocculation, the flocculation parameter (Figure 8B) and the shift in surface plasmon band (Figure 7) for 11-MUAM-functionalized gold sols are smaller than any other nanoparticles functionalized in this study. In the case of 8-PT-functionalized nanoparticles at high pH, the pyridine moiety is short of protons to generate intermolecular or interparticular H-bonding. The methylene chains are not well-packed (Figure 6A), and thus the carboxylates of residual TA are easier to expose to solution than those on 11-MUAM-functionalized nanoparticles. Taken together, the stability of 8-PT-functionalized gold sols is stable under high pH conditions, similar to that of 15-crown-5-S-functionalized gold sols.

Conclusion

By parallel comparison to MEA, MPA, and 11-MUDA, we have demonstrated the effectiveness of utilizing TA-stabilized nanoparticles as the intermediate for further functionalization. The substantial advantage of TA over the other thiols is the slow displacement rate, which allows the ω -functionalized thiols to build up steric stabilization in the second step. IR and XPS measurements verify the attachment of 11-MUDA, 15-crown-5-S, β -CD-S, 8-PT, and 11-MUAM. The films exhibit crystallinity for long chain thiols. Fractions of ω -functionalized thiols out of total thiols on nanoparticles are around 80% or higher, except for the 36% of the β -CD-S-functionalized case. Residual TA molecules are important in stabilizing nanoparticles at high pH. Plots of flocculation parameters against solution pH correlate the stable pH range with the surface functionality pretty well. At certain solution acidities, gold sols have difficulty carrying charges and appear flocculated. After being centrifuged and redissolved in suitable buffer solutions, the nanoparticles become dispersive, demonstrating the successful protection of the gold cores by steric stabilization.

Acknowledgment. We thank the National Science Council (ROC), National Tsing Hua University, and the Department of Chemistry for generous financial and research support. Thanks also to Dr. Y.-T. Tao for providing 8-PT.

Supporting Information Available: ¹H NMR spectra of β -CD-SH (Figure S1) and 11-MUAM (Figure S2), and photographs of 15-crown-5-S-modified (Figure S3) and 11-MUAM-modified (Figure S4) nanoparticles are available free of charge via the Internet at <http://pubs.acs.org>.

References and Notes

- (1) Elghamian, R.; Storhoff, J. J.; Mucic, R. C.; Letsinger, R. L.; Mirkin, C. A. *Science* **1997**, *277*, 1078–1081.
- (2) Liu, J.; Mendoza, S.; Roman, E.; Lynn, M. J.; Xu, R.; Kaifer, A. E. *J. Am. Chem. Soc.* **1999**, *121*, 4304–4305.
- (3) Reynolds, R. A., III.; Mirkin, C. A.; Letsinger, R. L. *J. Am. Chem. Soc.* **2000**, *122*, 3795–3796.
- (4) Boal, A. K.; Rotello, V. M. *J. Am. Chem. Soc.* **2000**, *122*, 734–735.
- (5) Mirkin, C. A. *Inorg. Chem.* **2000**, *39*, 2258–2272.
- (6) Kim, Y.; Johnson, R. C.; Hupp, J. T. *Nano Lett.* **2001**, *1*, 165–167.
- (7) Krasteva, N.; Besnard, I.; Guse, B.; Bauer, R. E.; Mullen, K.; Yasuda, A.; Vossmeier, T. *Nano Lett.* **2002**, *2*, 551–555.
- (8) Lin, S.-Y.; Liu, S.-W.; Lin, C.-M.; Chen, C.-h. *Anal. Chem.* **2002**, *74*, 330–335.
- (9) Nam, J.-M.; Park, S.-J.; Mirkin, C. A. *J. Am. Chem. Soc.* **2002**, *124*, 3820–3821.
- (10) Nath, N.; Chilkoti, A. *Anal. Chem.* **2002**, *74*, 504–509.
- (11) Vossmeier, T.; Guse, B.; Besnard, I.; Bauer, R. E.; Mullen, K.; Yasuda, A. *Adv. Mater.* **2002**, *14*, 238–242.
- (12) Obare, S. O.; Hollowell, R. E.; Murphy, C. J. *Langmuir* **2002**, *18*, 10407–10410.
- (13) Naka, K.; Itoh, H.; Chujo, Y. *Langmuir* **2003**, *19*, 5496–5501.
- (14) Sato, K.; Hosokawa, K.; Maeda, M. *J. Am. Chem. Soc.* **2003**, *125*, 8102–8103.
- (15) Brust, M.; Walker, M.; Bethell, D.; Schiffrin, D. J.; Whyman, R. *J. Chem. Soc., Chem. Commun.* **1994**, 801–802.
- (16) Templeton, A. C.; Wuelfing, W. P.; Murray, R. W. *Acc. Chem. Res.* **2000**, *33*, 27–36.
- (17) Chandrasekharan, N.; Kamat, P. V. *Nano Lett.* **2001**, *1*, 67–70.
- (18) Wuelfing, W. P.; Zamborini, F. P.; Templeton, A. C.; Wen, X.; Yoon, H.; Murray, R. W. *Chem. Mater.* **2001**, *13*, 87–95.
- (19) Brust, M.; Kiely, C. J. *Colloid Surf. A* **2002**, *202*, 175–186.
- (20) Sun, Y.; Xia, Y. *Science* **2002**, *298*, 2176–2179.
- (21) Quinn, B. M.; Liljeroth, P.; Kontturi, K. *J. Am. Chem. Soc.* **2002**, *124*, 12915–12921.
- (22) Gittins, D. I.; Susha, A. S.; Schoeler, B.; Caruso, F. *Adv. Mater.* **2002**, *14*, 508–512.
- (23) Sun, Y.; Xia, Y. *Adv. Mater.* **2003**, *15*, 695–699.
- (24) Miles, D. T.; Murray, R. W. *Anal. Chem.* **2003**, *75*, 1251–1257.
- (25) Hunter, R. J. *Foundations of Colloid Science*; Oxford University Press: New York, 1987; Vol. 1.
- (26) Napper, D. H. *Polymeric Stabilization of Colloidal Dispersions*; Academic Press: London, 1983.
- (27) Mulvaney, P. *Langmuir* **1996**, *12*, 788–800.
- (28) Link, S.; El-Sayed, M. A. *J. Phys. Chem. B* **1999**, *103*, 8410–8426.
- (29) Weisbecker, C. S.; Merritt, M. V.; Whitesides, G. M. *Langmuir* **1996**, *12*, 3763–3772.
- (30) Fujiwara, H.; Yanagida, S.; Kamat, P. V. *J. Phys. Chem. B* **1999**, *103*, 2589–2591.
- (31) Kamat, P. V. *J. Phys. Chem. B* **2002**, *106*, 7729–7744.
- (32) Aslan, K.; Perez-Luna, V. H. *Langmuir* **2002**, *18*, 6059–6065.
- (33) Frens, G. *Nat. Phys. Sci.* **1973**, *241*, 20–22.
- (34) Grabar, K. C.; Freeman, R. G.; Hommer, M. B.; Natan, M. J. *Anal. Chem.* **1995**, *67*, 735–743.
- (35) Flink, S.; van Veggel, F. C. J. M.; Reinhoudt, D. N. *J. Phys. Chem. B* **1999**, *103*, 6515–6520.
- (36) Gadelle, A.; Defaye, J. *Angew. Chem., Int. Ed. Engl.* **1991**, *30*, 78–79.
- (37) Zhu, M.; Schneider, M.; Papastavrou, G.; Akari, S.; Mohwald, H. *Langmuir* **2001**, *17*, 6471–6476.
- (38) Mayya, K. S.; Patil, V.; Sastry, M. *Langmuir* **1997**, *13*, 3944–3947.
- (39) Chen, S.; Kimura, K. *Langmuir* **1999**, *15*, 1075–1082.
- (40) Kumar, A.; Mandale, A. B.; Sastry, M. *Langmuir* **2000**, *16*, 6921–6926.
- (41) Mandal, S.; Gole, A.; Lala, N.; Gonnade, R.; Ganvir, V.; Sastry, M. *Langmuir* **2001**, *17*, 6262–6268.
- (42) Porter, M. D.; Bright, T. B.; Allara, D. L.; Chidsey, C. E. D. *J. Am. Chem. Soc.* **1987**, *109*, 3559–3568.
- (43) Kakiuchi, T.; Sato, K.; Iida, M.; Hobara, D.; Imabayashi, S.-i.; Niki, K. *Langmuir* **2000**, *16*, 7238–7244.
- (44) Collard, D. M.; Fox, M. A. *Langmuir* **1991**, *7*, 1192–1197.
- (45) Chidsey, C. E. D.; Bertozzi, C. R.; Putvinski, T. M.; Mujsce, A. M. *J. Am. Chem. Soc.* **1990**, *112*, 4301–4306.
- (46) Hostetler, M. J.; Templeton, A. C.; Murrar, R. W. *Langmuir* **1999**, *15*, 3782–3789.
- (47) Hostetler, M. J.; Green, S. J.; Stokes, J. J.; Murrar, R. W. *J. Am. Chem. Soc.* **1996**, *118*, 4212–4213.
- (48) Ingram, R. S.; Hostetler, M. J.; Murrar, R. W. *J. Am. Chem. Soc.* **1997**, *119*, 9175–9178.
- (49) Lee, T. R.; Carey, R. I.; Biebuyck, H. A.; Whitesides, G. M. *Langmuir* **1994**, *10*, 741–749.
- (50) Johnson, S. R.; Evans, S. D.; Brydson, R. *Langmuir* **1998**, *14*, 6639–6647.